Overview of the FTU results

V. Pericoli-Ridolfini, A. Alekseyev[1], B. Angelini, S.V. Annibaldi, M.L. Apicella, G. Apruzzese, E. Barbato, J. Berrino[2], A. Bertocchi, W. Bin[2], F. Bombarda, G. Bracco, A. Bruschi[2], P. Buratti, G. Calabrò, A. Cardinali, L. Carraro[3], C. Castaldo, C. Centioli, R. Cesario, S. Cirant[2], V. Cocilovo, F. Crisanti, G. D'Antona[4], R. De Angelis, M. De Benedetti, F. De Marco, B. Esposito, D. Frigione, L. Gabellieri, F. Gandini[2], E. Giovannozzi, G. Granucci[2], F. Gravanti, G. Grossetti[2], G. Grosso[2], F. Iannone, H. Kroegler, V. Lazarev[1], E. Lazzaro[2], M. Leigheb, L. Lubyako[5], G. Maddaluno, M. Marinucci, D. Marocco, J.R. Martin-Solis[6], G. Mazzitelli, C. Mazzotta, V. Mellera[2], F. Mirizzi, G. Monari, A. Moro[2], V. Muzzini[2], S. Nowak[2], F. Orsitto, L. Panaccione, M. Panella, L. Pieroni, S. Podda, M. E. Puiatti[3], G. Ravera, G. Regnoli, F. Romanelli, M. Romanelli, A. Shalashov[5], A. Simonetto[2], P. Smeulders, C. Sozzi[2], E. Sternini, U. Tartari[2], B. Tilia, A.A. Tuccillo, O. Tudisco, M. Valisa[3], A. Vertkov[7], V. Vitale, G. Vlad, R. Zagórski[8], F. Zonca

Associazione Euratom-ENEA sulla Fusione, C.R. Frascati, 00044, Frascati, Roma, Italy
e-mail contact of main author: pericoli@frascati.enea.it

Abstract. Steady internal transport barriers (ITB) are obtained in FTU almost full non-inductive current drive (CD) discharges at ITER relevant magnetic field and density ($n_{e0} \geq 1.3 \cdot 10^{20}$ m^{-3}). The heating power is to electrons with no momentum input similar to ITER condition. Two RF systems, lower hybrid (LH) and electron cyclotron (EC), provide the CD and power sources. The energy confinement time exceeds the ITER 97-L scaling by about 1.6 times. The barrier dynamics is unaffected by ion collisional heating: turbulence is strongly suppressed and the ion transport remains at the ohmic level. ITB radius on FTU can be varied between $0.2 \leq r/a \leq 0.65$ modifying the LHCD deposition profile and the safety factors q or via ad hoc use of co/counter ECCD. Feedback control/suppression of MHD tearing modes (TM, m=2) with EC waves relies on a real-time detection of the TM and of its radial location. A liquid lithium limiter (LLL) of novel design, composed of a mesh of porous capillaries, has been tested successfully for the first time on a medium size tokamak. The LLL surface showed no damage up to the maximum thermal load of 5 MW/m^2. With LLL cleaner plasmas are obtained and the particle recycling strongly drops; new interesting regimes of particle transport arise at high density. Progress on disruption mitigation by means of EC power has been made. Testing the collective Thomson scattering in ITER-relevant configuration has stressed that avoiding backscattered radiation to the source is very crucial. The theory of the evolution of fishbone-like instabilities driven by LH generated supra-thermal electrons in FTU is outlined, and its relation to the trapped α particles dynamics is stressed.

1. Introduction

FTU is a compact high magnetic field tokamak (major radius R=0.93 m, minor radius a=0.3 m, toroidal magnetic field $B_T \leq 8$ T, plasma current $I_p \leq 1.6$ MA) aimed at developing advanced scenarios at magnetic field and densities relevant to ITER operation, as well as its supporting physics [1]. The FTU auxiliary heating systems, lower hybrid (LH, frequency f_{LH}=8 GHz, power $P_{LH} \leq 2$ MW) and electron cyclotron (EC, f_{EC}=140 GHz, power $P_{EC} \leq 1.6$ MW) waves, heat electrons (e^-) and inject no momentum. As in ITER, ions (i^+) are heated only by e^--i^+ collisions.

Since the last FEC [2], the main hardware upgrades have been the installation of a system for real time MHD mode detection and control by EC heating (ECH), of a new liquid lithium limiter

[1] TRINITI, Troitsk, Moscow reg., Russia
[2] Associazione EURATOM-ENEA, IFP-CNR, Via R. Cozzi, 53 - 20125 Milano, Italy
[3] Consozio RFX, Corso Stati Uniti 4, I-35100, Padova, Italy
[4] Politecnico di Milano, Piazza Leonardo Da Vinci 32, 20133 Milano, Italy
[5] Institute of Applied Physics, Russian Academy of Science, Nizhny Novgorod, Russia
[6] Universidad Carlos III de Madrid, Avenida de la Universidad 30, 28911 Madrid, Spain
[7] FSUE, "RED STAR", Moscow, Russia
[8] Institute of Plasma Physics and Laser Microfusion, EURATOM Association, 01-497, Warsaw, Poland

(LLL) that has broadened the FTU capability of studying plasmas with different wall conditions, and of a new motional Stark effect and charge exchange recombination spectroscopy (MSE/CXRS) diagnostic, presently being commissioned, to provide information on the safety factor, q, and ion temperature profiles. A collective Thomson scattering system in the microwave frequency range (f=140 GHz) has been tested for the first time in an ITER-like configuration. A LH multijunction launcher has been also tested, reaching a power density of 8 kW/cm^2 at 8 GHz.

In this paper, the main new results from the FTU experimental campaigns will be presented starting from the insights gained in the advanced tokamak scenarios, Sect. 2, followed by the results in the active control of the magnetohydrodynamic (MHD) instabilities with the EC power, Sect. 3. In Sect. 4 we will describe the result obtained with LLL. Theoretical understanding of the electron fishbones instability dynamics will be presented in Sect. 5. Finally in Sect. 6 the activity in support of ITER (disruption mitigation, study of LH disruptions, CTS diagnostic test and physics studies) will be summarized together with the results on the physics of LH propagation. A short summary of the perspective for the years 2006-2008 will be given finally in sec. 7.

2. Advanced Tokamak Scenarios

The aspect more relevant to an ITER like internal transport barriers (ITB) addressed by the FTU program concerns influence of the high density and electron-ion collisional coupling on the mechanisms that produce the e$^-$ITBs, The possibility to verify if an ion transport barrier could develop in presence of e$^-$ heating only would be very important to clarify the role of the many mechanisms candidates to stabilize the ion turbulence. Conversely, FTU cannot deal with questions such as stability at high ß$_p$ (ß$_p$=2μ$_0$<p>/<B$_{pa}$>^{2} is the poloidal beta, μ$_0$=vacuum magnetic permeability, <p> average plasma pressure, <B$_{pa}$> average poloidal field strength at the plasma boundary), due to its high magnetic field, the role of fast particles and the divertor physics, FTU being a limiter device. Further details on FTU can be found in Ref. [1].

Stationary ITB regimes, candidates as a steady scenario for ITER, have been established in almost full current drive (CD) conditions at the ITER working density and magnetic field, B$_T$. A previous work [3] reported on the high density steady ITBs, with the central density $n_{e0} \geq 1.3 \cdot 10^{20}$ m^{-3} ($n_{e0}/n_{GW} \geq 0.9$, n_{GW}=Greenwald value [4]. and electron temperature $T_{e0} \geq 5$ keV. The energy confinement time is enhanced by 1.6 times respect to the ITER97-L scaling, applicable to FTU, and ion collisional heating does not affect the barrier dynamics. The barrier was however not wide. Since the last FEC, methods to control the barrier radial width by LH current drive (LHCD) have been successfully developed, even though limited so far to lower density regimes. Steady ITB radii up to $r/a \leq 0.67$ have been obtained by peripheral LH absorption, favored primarily by operation at low safety factors q [5]. The time traces of the most relevant parameters of a steady wide barrier are presented in Fig. 2.1

The usual q(r) shape in an ITB has a central value $1<q_0<2$, followed by a low or even weakly inverted magnetic shear region with $q_{min} \approx 1.2$-1.3 (shear is defined as $s=r/q \cdot dq/dr$) at the end of which is located the ITB foot, generally close to $q_{min} \approx 1.5$ [6]. If $r_{ITB} \approx a/2$ the q(r) profile resembles that of typical hybrid regimes [7]. The link in FTU of the ITB foot with a low-order rational q-value surface agrees well with JET observation [8], despite the quite different ITB genesis. These are obtained at JET, and also at JT60-U [9], with a very early heating or CD not allowed in FTU by various constraints [10], when q(r) is very far from the relaxed shape and show remarkably reversed shears and $q_{min}>2$.

The EC power is mainly used to heat (ECH) inside the barrier to benefit of the reduced energy transport. This in turn reinforces the barrier: the electron temperature gradient increases improving further the energy confinement as illustrated previously [6]. EC current drive (ECCD) is often a precious auxiliary tool either in co- or counter (ctr-) configuration in building the proper current profile. In the case of Fig. 2.1 co-ECCD slightly off-axis ($r_{ECCD} \sim 0.2 \cdot a$,

r_{ECCD}=minor radius of the ECCD deposition) facilitates steadiness, whereas on-axis ctr-ECCD is necessary for building high density ITBs, $\bar{n}_e \approx 10^{20}$ m^{-3} [11, 10].

The ITB energy confinement improves with the barrier strength, but tends to saturate for strong ITBs, as shown in Fig. 2.2. Here we plot the enhancement factor $H_{97\text{-}L}=\tau_E/\tau_{E97\text{-}L}$ versus $\rho^*_T=\rho_{L,s}/L_T$ (τ_E=experimental energy confinement time, τ_{E97}= ITER97-L scaled value of τ_E, $\rho_{L,s}$=Larmor radius of the ions with the sound velocity is normally assumed as a measure of the barrier strength, and $L_T=T_e/(dT_e/dr)$). Clearly the improvement improves very rapidly close to the threshold value $\rho^*_{T,th}=0.014$ [10], and seems to saturate at $H_{97\text{-}L}\approx 1.7$. The best confinement pertains to points with ECH. The quite high correlation degree between $H_{97\text{-}L}$ and ρ^*_T leaves little weight to the barrier width. This is not surprising if the ITB is modeled as a high confinement core, with a defined confinement time τ_h, surrounded by a poor confinement region. The additional power P_h deposited inside the core would raise its energy and consequently that of the entire plasma by the amount $P_h \cdot \tau_h$, irrespective of its width.

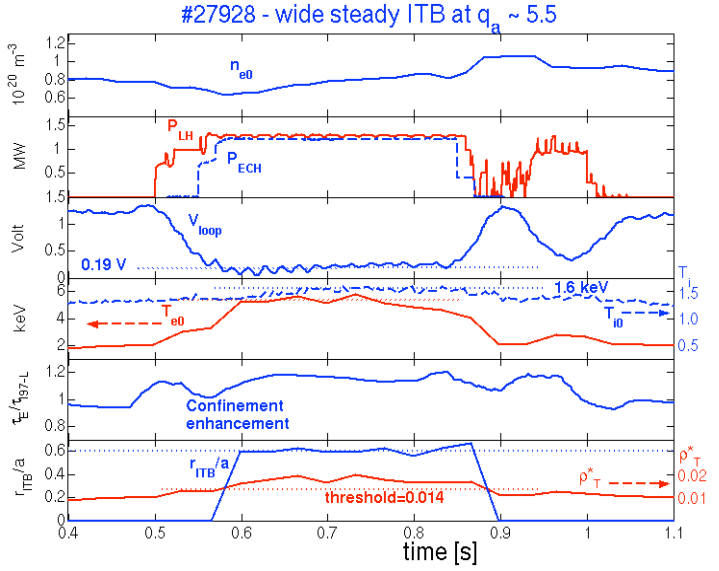

FIG. 2.1 - Time evolution of the most significant parameters for #27928, the widest steady ITB; co-ECCD configuration slightly off axis (≈6 cm). I_p=0.51 MA, B_T=5.3 T, q_a≈5.5

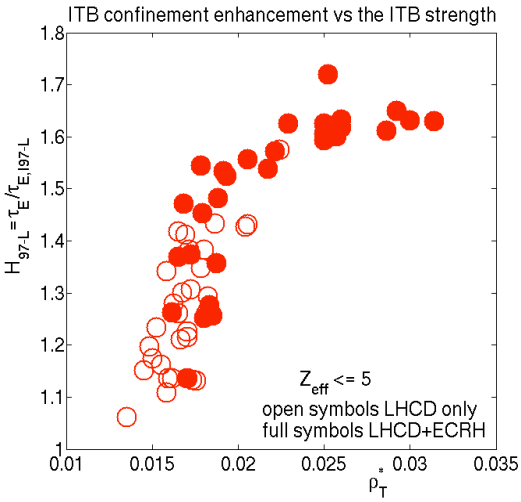

FIG. 2.2 - Global energy confinement of the ITBs, shown as the enhancement over the ITER97-L scaling versus the barrier strength

The ion thermal transport slows down inside the ITB, according to the JETTO code transport analysis supported by the measured ion temperature profiles $T_i(r)$. The heat conductivity, χ_i, drops below the neoclassical value reaching the ohmic neoclassical level. This happens for both narrow and wide ITBs just where the ITB foot is located. This is shown in Fig. 2.3 where $\chi_i(r)$ computed from experimental $T_i(r)$ (from neutron measurements) and calculated (from neoclassical transport theory) is plotted for the two steady discharges here considered, the highest density (#26671) and the widest ITB (#27928). The double traces limit the variability range of χ_i during the ITB evolution phase. The computed levels are quite close to the neoclassical values of OH discharges with similar parameters. The importance of such result, though limited so far at low value of T_{i0}, is relevant for the physics of the turbulence stabilization of the ion and electron channels. It suggests that the same mechanisms responsible for the reduced electron transport, i.e. a proper low shear q profile, affect favorably also the ion transport, without the support of induced plasma rotation. Turbulence characterization of such regimes shows a clear drop of the overall fluctuation level close to the barrier foot and a decorrelation of the modes with $k_\theta \rho_i \approx 0.3$ [6, 12], which is in the right range for affecting both e^- and i^+ transport channels.
In exploring the advanced scenarios in different plasma regimes we tried also to extend the potentialities of the EC power beyond the resonance conditions on thermal electron, studying

direct absorption on the LH generated fast electrons. Significant synergy between LH and EC is indeed found in the EC downshifted absorption, when the relativistic e^- mass increase is balanced by an equal relative increase of B_T. The EC waves are effectively absorbed, more than 80% of the EC power, and the CD efficiency gained by the tails is comparable to the LH values. This is shown in Fig. 2.4 where the CD efficiencies obtained with EC absorption onto LHCD suprathermal electrons (SECCD) are plotted versus the volume averaged electron temperature together with data points of the FTU LHCD database. The SECCD efficiencies compare well to these latter despite they are underestimated because the overall injected power LH+EC is taken into account neglecting the lost EC power fraction. More details can be found in Ref. [13].

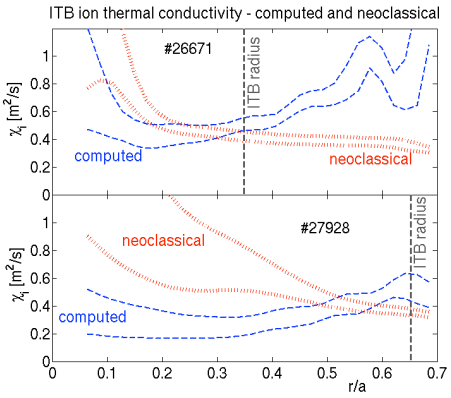

FIG. 2.3 - Ion thermal conductivity the highest density (top) and the widest (bottom) steady ITB. The lines, dotted or dashed, limit the variability range during the whole ITB phase.

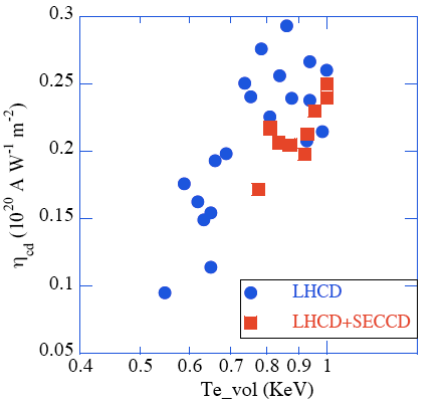

FIG. 2.4 - FTU current drive database vs. volume averaged T_e. LHCD and EC power are within 0.7 – 1.2 MW for SECCD data.

3. MHD mode control.

The absorption of EC waves is very localized on a tokamak and hence can directly affect the helical currents sustaining the Tearing Mode (TM) MHD instability, leading to its suppression. The automation of the stabilizing action, needed in a fusion reactor, can be achieved by a "smart EC Waves launcher" capable of reliable and fast reaction to MHD, by zeroing the distance between the island position r_{island} and the deposition radius r_{dep} [14].

The measure of r_{island} can be performed by a spatially resolved measurement of T_e oscillations (ECE radiometer is the best option) naturally induced by the TM rotation. The π phase jump on opposite sides of the island can be used in principle to locate r_{island}. In practice, the island is located where a minimum correlation in adjacent ECE channels is observed [15]. In order to increase robustness of r_{island} detection against noise and sawteeth influence, a Mirnov coil provides a reference signal for a dynamic ECE filtering around TM frequency.
Th r_{dep} measurement is usually accomplished by modulating the EC power and looking for the peak in synchronous T_e oscillations. In the case of multiple beam applications, each r_{dep} can be distinguished by a different modulation frequency [14].

In FTU experiments we demonstrated the impact of ECH on MHD of coupled modes [16], stabilized TMs by properly aligned ECH [17], and finally achieved automatic stabilization [18].

The technique used to localize a MHD mode is shown in Fig. 3.1 as the correlation between adjacent ECE channels of a 12-channels polychromator, and the correlation between each ECE and a Mirnov coil signals. ECE_i/ECE_j correlation shows a clear minimum at ch.9/ch.10. Correspondingly, ECE/Mirnov correlation changes sign from ch.9 to ch.10. A (2,1) mode, as confirmed by soft X-ray tomography, is unambiguously located between ch.9 and ch.10.

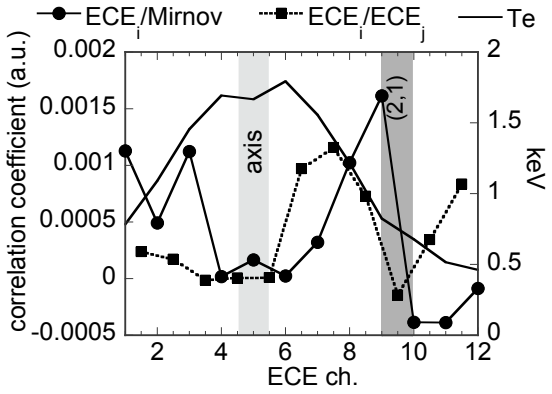

FIG. 3.1 - Correlation coefficient (without normalization) between nearby ECE channels (squares) and between ECE and Mirnov coil signals (dots). The electron temperature profile is shown for reference

Two gyrotrons (G1 and G3) are used for these experiments. Their power is absorbed in a position corresponding to ECE ch.7 (G1) and to ch.10 (G3). In order to allow r_{dep} detection, G1 is modulated at 250 Hz, and G3 at 300 Hz. The duty cycle is normally low in "watch mode", i.e. it is modulated at low average power only for r_{dep} detection. During stabilization, r_{dep} monitoring is continued by complementary modulation at high average power.

Figure 3.2 shows the results of two real time stabilization experiments. In the discharge of frame a) an internal disruption destabilizes the (2,1) mode at t≈0.56 s. After 20 ms of integration time, the mode is recognized and located between ECE ch.9 and ch.10 (see also Figure 2.1). G3, absorbed in the position corresponding to ECE ch.10 is switched to high duty cycle, while the other continues unchanged. After ≈100 ms stabilization is completed and G3 returns to low average power. In frame b), the mode is destabilized when the EC stabilization system is not yet enabled. However, mode recognition is active and G3 is switched to high average power as soon as the automatic control is enabled.

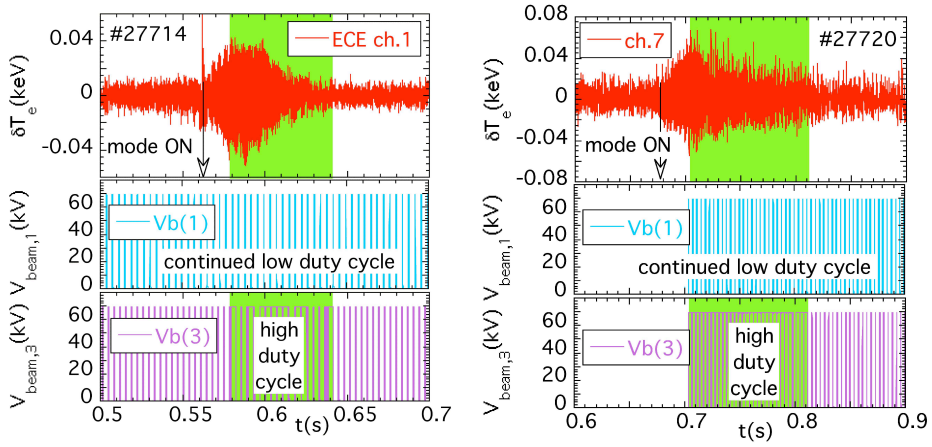

FIG. 3.2 - Stabilizing effect of ECH in two different discharges. Top to bottom: oscillation in the T_e observed in one ECE channel, the beam voltage applied to gyrotron G1 and G3. EC power from the two gyrotrons is absorbed at two different radii

4. The Liquid Lithium limiter (LLL).

The interest on liquid lithium as a first wall material for magnetic fusion devices is incessantly growing in the world tokamak community. In the USA, extensive experimental, on CDX-U and DIII-D, and modeling work is being carried, in the framework of the US Advanced Limiter-divertor Plasma-facing Systems (ALPS) [19]. Indeed, Li liquid divertor targets could have an unlimited lifetime, due to the possibility of continuously supplying from outside a low temperature liquid (the Li melting point is 180.5 °C), therefore reducing strongly the problem of erosion by thermal overloads, either transient or steady. Li is also more appealing for coating the main chamber walls of a reactor than the currently envisaged Be.

ENEA and two Russian laboratories, TRINITY & REDSTAR, started a joint program some years ago that, at the end of 2005, led to test a LLL of new design for the first time in a high field, medium size, carbon free tokamak (FTU). The design novelty rests on the capillary porous system (CPS) configuration [20]. A mesh of capillary channels is fed with liquid Li by an underlying reservoir and the associated surface tension withstands the electromagnetic tearing-off forces due to the JxB effect.

Here we summarize the main successful technical tests so far completed on the LLL and describe the principal physical effects observed on the plasma behavior, edge and core, due to LLL. This first experimental campaign has been limited to ohmic plasmas, whose main parameters range within $0.5 \leq I_p \leq 0.9$ MA, line averaged density $0.2 \leq \bar{n}_e \leq 2.6 \cdot 10^{20}$ m^{-3}, B_T=6T. More details can be found in [21, 22]

4.1 Technical achievements with LLL

Lithization (i.e. Li coating) of the FTU walls is carried out by inserting the LLL 1-1.5 cm within the SOL in the vessel bottom during plasma discharges. Thermal load, which can raise the surface LLL temperature from the base value of ~200 °C to ~450 °C, and particle sputtering pull gaseous Li out the CPS edge. SOL transport mechanisms spread then it over the whole first wall surface, vessel + toroidal limiter (made by the Mo-based alloy TZM). An almost complete Li coating is achieved after two or three plasma discharges and it is marked by the absolute predominance in the UV emission spectrum of the Li-III line at 13.5 nm with respect to the usual lines of O, Mo and Fe that drop to a negligible level, about 4-5 times lower than the Li-III line.

The LLL has been exposed to thermal loads in excess to 5 MW/m^2 without any damage of the lithium surface or phenomena as “lithium bloom”. The maximum increase of temperature on Li surface has not exceeded 250 °C also for the strongest interaction with the plasma, suggesting the onset of some sort of self-protection mechanism [22].
In describing the physics effects distinction is made between those linked to the wall lithization and those more strictly caused by the actual presence of the LLL in the scrape-off layer (SOL) plasma, with consequent strong mutual interaction. The SOL observations are interpreted in the frame of the 2D edge physics code TECXY [23].

4.2 Effects of the lithized walls

With “lithized” walls the plasma appears remarkably cleaner: loop voltage, radiated power and Z_{eff} are lower [24]: practically no impurity but lithium is seen on the UV spectra. The strong lithium pumping action highly reduces the D_2 recycling and allows a tight control of the density in the range $0.15\text{-}2.6 \cdot 10^{20}$ m^{-3}. The upper density value is a factor 1.4 above the Greenwald limit, while the lower density value was never attained in FTU before.

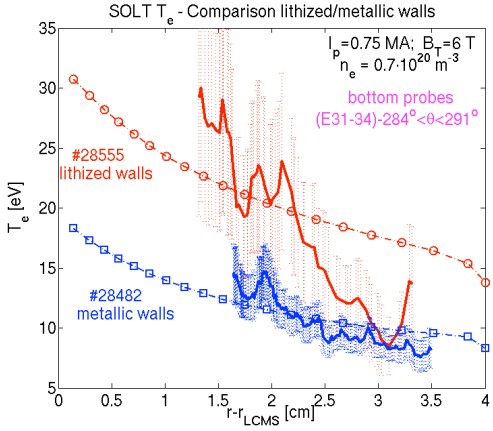

FIG. 4.1 - $T_e(r)$ in the SOL for metallic and lithized walls. Experiment: full lines (errors as shadowed band). Simulation: dashed lines +symbols. TECXY still has not tightly reproduced $\lambda_{T,\,Li}$

The most interesting change in the SOL parameter is the temperature increase, illustrated in Fig. 4.1 for I_p=0.75 MA. Measurements are from a reciprocating Langmuir probe in the vessel bottom and are averaged over a poloidal angle $\Delta\theta \sim 9°$. The amount of gas puffed and the power entering the SOL, $P_{SOL} \sim 0.5$ MW, are quite similar. The SOL density remains almost unchanged. TECXY can reproduce the unusual (for FTU) quite large ΔT_e (~10 eV, almost 50%) only if: i) H recycling is almost neglected as a consequence of the strong pumping effect of the Li coating; ii) a small

Mo contribution to the SOL radiation losses is maintained to avoid obtaining a much higher T_e value. This Mo residue could come from the not fully Li coated toroidal limiter. So far TECXY could not fully reproduce the temperature radial decay with lithization within the usual parameter ranges. Apparently, the heat diffusion coefficient slightly affects the profiles that are mainly determined by parallel transport and by recycling.

4.3 Effects of the LLL inside the vacuum vessel

The LLL surface represent a strong localized source of Li atoms and ions that can deeply modify the SOL properties and those of the core plasma, due to the additional large particle pumping capability and to the radiation losses. According to TECXY code, a poloidally delimited region inside the SOL between LLL and the toroidal limiter should form with strongly enhanced radiation, increased density and lower temperature. CCD camera pictures of the plasma discharge and measurements with both reciprocating and fixed (on LLL) Langmuir probes do confirm this.

The most interesting effect of the presence of the LLL inside the vessel is seen in high density discharges, when $\bar{n}_e > 0.5 \cdot n_{GW}$, where the large recycling drop can deeply change the whole SOL dynamics and affect heavily also the core plasma properties. An enlightening example is given by comparing the time evolution of two very time close discharges, #28508 and #28510. In #28510 the LLL is inserted 1.4 cm inside the vacuum vessel, whereas in #28508 it is left outside. In fig. 4.2, the line densities are plotted in frame a) together with the Greenwald limit. Frame b) shows the H_α light emission seen by one of the horizontal array detectors (all the others show a very similar behavior); frame c) gives the density peaking factor $f_{pk}=n_{e0}/\langle n_e \rangle$, ratio of the central to the volume averaged density value.

With LLL (#28510) a new regime is built at t=0.3 s that lasts about 0.5 s with the following features. 1) $\bar{n}_e$ grows up to $2 \cdot 10^{20}$ m^{-3} ($\sim n_{GW}$), twice the pre-programmed value, which is just that maintained in #28508, and remains almost constant, despite no gas is fuelled into the vessel. 2) The H_α light drops as in L-H transitions in divertor plasmas and remains low, indicating a strongly reduced H particle recycling, whereas in #28508 the H_α detectors' signals saturate. 3) The density peaking raises from $f_{pk} \sim 1.5$ in #28508 up to $f_{pk} > 2$ in #28510.

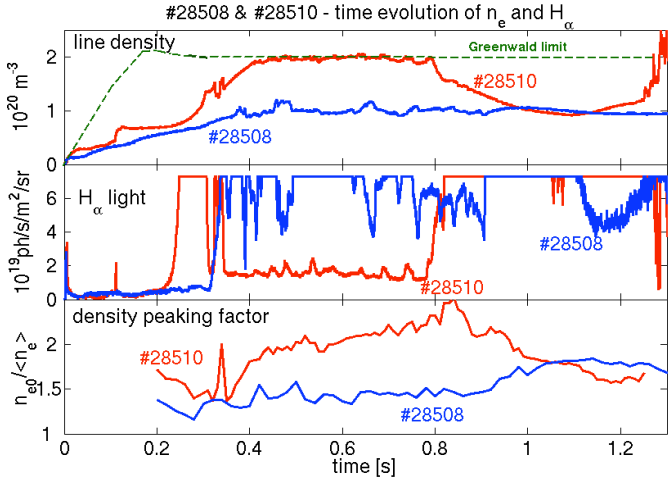

FIG. 4.2 – Comparison of line density (top), H_α light intensity (middle) and density peaking factor (bottom) for two identically pre-programmed high-density discharges. #28510: LLL inserted ~1.4 cm in the SOL; #28508: outside

This is a quite high value when $\bar{n}_e$ is so close to n_{GW} and contrasts with the common observation of flatter density profiles as n_e grows. For the whole duration of this phase a clear steepening of $n_e(r)$ occurs close to the edge (r/a~0.7) [21] resembling the peculiar feature of barrier. However, despite the large slowing down of the outward particle radial transport [21] the energy confinement does not show a clear increase, even if it is at the top values so far obtained in FTU in the relevant range of parameters

5. Theoretical analyses of electron-fishbone dynamics

An example of the significant and positive feedback between theory and experimental observations is the explanation of the processes underlying the excitation of fishbone-like internal kink instabilities driven by supra-thermal electrons. A detailed theoretical analysis of these modes

is given in Ref. [25], along with an interpretation of the experimental results, which have strongly motivated this study. The peculiarity of FTU observations with respect to previous and similar ones (see, e.g., Ref. [26]), where the supra-thermal electron tail was associated with high field side ECRH, is the excitation of electron-fishbones in the presence of LH power injection only [27]. Due to the frequency gap in the low-frequency shear Alfvén continuous spectrum for modes propagating in the ion diamagnetic direction, effective electron-fishbone excitation favors conditions characterized by supra-thermal electron drift-reversal, consistently with experimental observations [26, 28]. For the same reason, the spatial gradient inversion of the supra-thermal electron tail is necessary, explaining why ECRH excitation is observed with high field side deposition only [26, 28]. The case of mode excitation by LH only [27] follows the same physics with few additional twists. The fast electron populations that effectively excite the mode are the trapped and barely circulating particles. Meanwhile, LH power forms a perpendicular fast electron tail, which is moderately slanted towards the counter-current direction; i.e., despite that it guarantees the inverted spatial gradient of the supra-thermal tail, it is less selective than high field side ECRH in producing particles with drift-reversal. Thus, in the case of mode excitation by LH only, the presence of circulating supra-thermal particles is crucial for two reasons: (i) barely circulating particles effectively contribute to the mode excitation; (ii) well circulating particles modify the current profile, eventually reversing the magnetic shear and broadening the fraction of trapped particles characterized by drift reversal.

As in the case of ion-fishbones [29], two branches of the electron-fishbone exist: a discrete gap mode and a continuum resonant mode. The latter does not generally require neither drift-reversal nor inverted spatial gradient of the supra-thermal tail; however, it has a higher excitation threshold and, thus, it is unfavored, particularly for the branch propagating in the electron diamagnetic direction.

The two modes, excited on FTU under different levels of LH power inputs, appear on (fast) electron temperature fluctuations with very distinctive signatures (see Fig. 5.1). Characterizing the nonlinear physics of electron-fishbones: during high power LH injection, an evident transition in the electron-fishbone signature takes place from almost steady state nonlinear oscillations (fixed point) to regular bursty behavior (limit cycle). Ref. [25] discusses a simple yet relevant nonlinear dynamic model for predicting and interpreting these observations.

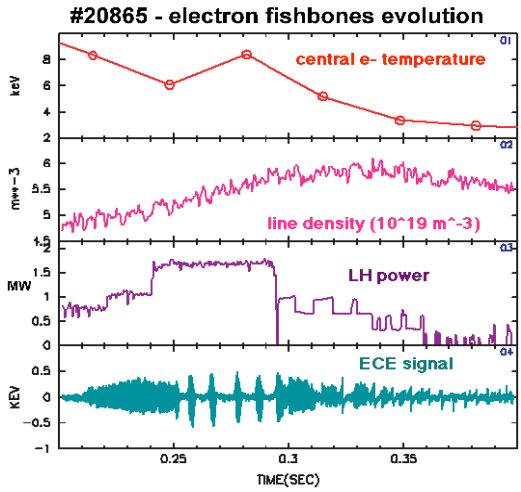

FIG. 5.1 - Time evolution of thermal e^- temperature (01), plasma density (02), LH power input (03) and (fast) e^- temperature fluctuations (04). It is clear that the nonlinear behavior of these latter (electron-fishbone) reflects the level of LH power

The most interesting feature of e^- fishbones is their relevance to burning plasmas. In fact, unlike fast ions in present day experiments, fast electrons have small orbits, which do not introduce additional complications in the physics due to non-local behaviors, similarly to α particles in reactor relevant conditions. Meanwhile, the bounce averaged dynamics of both trapped as well as barely circulating electrons depends on energy (not mass): thus, their effect on low frequency MHD modes can be used to simulate/analyze the analogous effect of charged fusion products. Moreover, the combined use of ECH and LH provide extremely flexible tools to investigate various nonlinear behaviors, of which FTU experiment provides a nice and clear example (Fig. 5.1).

6. Supporting physics studies

FTU experiments have also been devoted to some specific ITER issues and to interpret the LHCD physics. On the ITER side the following items were addressed: disruption mitigation by

means of EC power, study of disruptions during LH, and reliability analysis of the microwave (140 GHz) collective Thomson scattering (CTS) diagnostic in the configuration proposed for ITER. On the LHCD side the statistical analysis of the CD efficiency has been performed and the modeling of linear and non-linear interaction of the LH waves with the edge plasma has been started.

6.1. Disruption mitigation with ECH and LH disruptions

Experiments have been performed in deuterium plasmas in order to study disruption avoidance by ECH. The power has been applied during the current or energy quench of disruptions triggered either by injection of Mo through laser blow-off in 0.5 MA discharges or by pre-programming the gas puff feedback system to provide $\bar{n}_e$ above the density limit (~1.2×10^{20}m^{-3}) in 0.36 MA discharges. The EC power (up to 3 gyrotrons P_{EC}=1.2 MW) has been injected on-axis or off-axis (O-mode, perpendicular direction) and triggered by the V_{loop} signal exceeding a preset threshold [30]. In the case of Mo-injection, ECH has been applied before the onset of strong MHD activity (Fig. 6.1) and disruption avoidance has been found to occur with off-axis ECH deposition. The results of a power deposition scan are presented in Fig. 6.2 (P_{EC} = 0.4÷1.2 MW): the disruption is avoided only when the power is absorbed close to the q=2 surface (as inferred from MHD measurements) and stabilization of m/n=2/1 and/or 3/1 modes is observed.

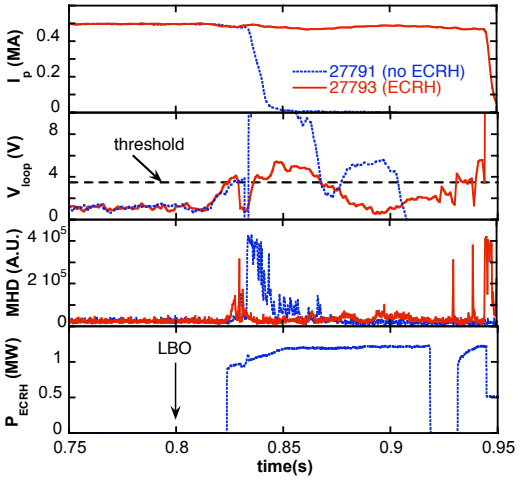

FIG 6.1 - Mo-injection disruptions: time traces of I_p, V_{loop}, MHD activity (B_{pol}) and EC power.

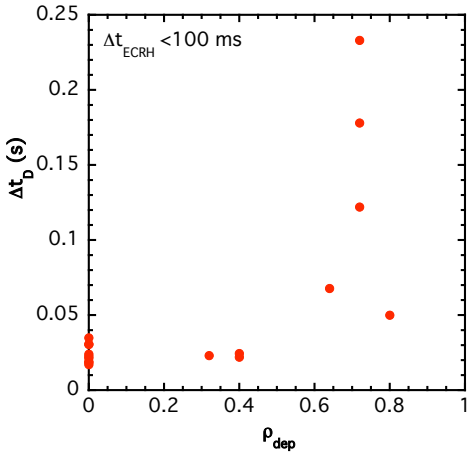

FIG 6.2 - Scan of ECH deposition radius in Mo-injection disruptions; the difference Δt_D is the delay of the I_p null from the start time of the MHD mode

No avoidance is attained nor delayed current quench is observed with central deposition. In the few density limit experiments carried out so far (due to operational problems caused by the EC cut-off at high density), disruptions have been avoided with central deposition (P_{EC}=0.8 MW) even after the start of a considerable MHD activity. The gas puffing causes a progressive cooling of the edge that changes the current profile and increases the 2/1 mode. This causes a first mini-disruption with a consequent slowing down of the 2/1 rotation frequency while a more internal 3/2 mode, at 7 kHz, appears. A flattening of the q profile (sawteeth disappear) occurs before the disruption, while central ECH absorption, reheating the core, peaks the current profile restoring the sawtooth and reducing the 3/2 mode amplitude. Off-axis (r/a=0.7) ECH absorption has not been found effective, but the absorbed power was very poor (10%) due to the low temperature. Experiments are in progress to optimize the timing and absorption radius of the EC power.

In FTU both ECH and LH can quench a runaway population [31], if this pre-exists to the heating pulse, by lowering the toroidal electric field below the threshold for generating runaways [32]. However, in case of LHCD, the suprathermal electron population produces further runaways

once LHCD is over (if plasma conditions allow it) due to acceleration by the restored electric field. In a similar way, in disruptions occurring during LHCD, large runaway currents (up to 80% of the pre-disruption I_p) can be produced. The largest runaway currents correspond to the slowest current decay rates. This is consistent with the acceleration of pre-existing LH-generated suprathermal electrons during the disruption current quench [33], while cannot be explained through the Dreicer and avalanche mechanisms of electron thermal runaway generation. Such results can be relevant for the operation of ITER whenever LH power is used.

6.2. Collective Thomson Scattering (CTS) diagnostic studies

The ITER relevance of the CTS experiment in FTU lays in the wave propagation at frequency below gyro-resonance, f_{gyr}=140 GHz, $195 \le f_{EC} \le 220$ GHz. Indeed, a recent feasibility study [34] clearly stated that the diagnostic of the confined alphas in ITER based on mm-wave CTS requires f_{gyr}=50-60 GHz, with propagation in the X-mode, with $f_{ec,ITER}$~151 GHz ($B_{T0,ITER}$~5.4T). Interesting results followed the unambiguous interpretation in 2006 of strongly anomalous non-thermal spectra systematically observed. Here we limit to summarize the most relevant facts, while a dedicated paper on the subject is being published [35].

The anomalous spectra, a typical example of which is shown in Fig. 6.3, were detected with both aligned- and in misaligned-antenna. The spectral power is several orders-of-magnitude higher than predicted for the ion-thermal feature, 0.5 keV against the detected 70 keV of Fig. 5.3. Moreover, this spurious signal should be about 5 orders of magnitude higher at the origin, since is collected after multiple wall reflections and therefore subject to antenna decoupling (~50 dB).

Attempts of explaining this anomaly in terms of plasma-wave processes soon failed. On purpose tests with shots performed in absence of plasma with the signal picked-up directly from the transmission line, hence before the wave beam enters the plasma, revealed that the anomalous spectra were still produced provided a toroidal magnetic field was applied. It was then realized that back-reflections could perturb the gyrotron and modify the launched spectrum, which is in turn collected as stray-radiation independently of the CTS geometry. The possible effects of resonances and cutoffs in causing unexpected partial back-reflection of the beam power were then investigated. In the CTS configuration, $f_{gyr} < f_{ec}$, an electron cyclotron, an upper hybrid layer, and the right-handed cutoff for the X mode (XM) are unavoidably crossed by the probe beam in its path to the plasma. In these conditions whenever a mode mixture is injected, as in our case, the power fraction in the X mode can be effectively reflected at the cutoff, provided the beam itself converts the critical layers from latent to active by exciting a breakdown plasma.

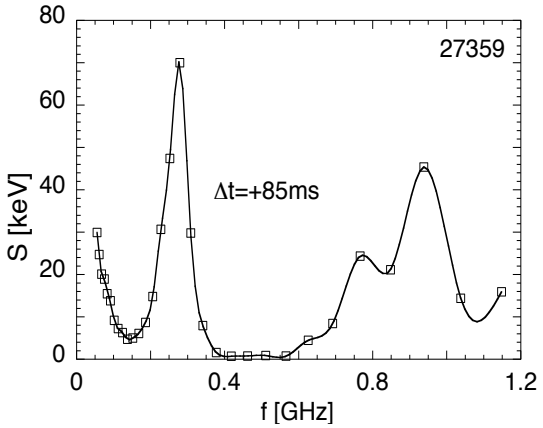

FIG. 6.3. - Typical anomalous spectrum with a relatively weak low-frequency feature and strong spectral lines at low and high frequency. Pulse length: 380 ms; integration time: 30 ms. B_{T0}=7T, P_{gyr}=307kW, $\bar{n}_e = 0.75 \cdot 10^{20} m^{-3}$, T_{e0}=2 keV

Reconstruction of the field isolines showed that the EC layer was near to the port mouth. At the end of the campaign, antenna inspection further showed that wakes were present on the last two antenna-mirror surfaces [35] at the location and with the inclination proper of the standard field (B_T=7 T). Even though our particular layout may have contributed to strengthen the gyrotron perturbation, the large number of other potential candidates strongly suggests forcing the critical layers to remain in any case latent.

The most viable of the solutions considered so far seems a remote-steering antenna (RSA) [36] with a vacuum tight ceramic (or diamond) window at its mouth on the plasma side. A RSA of special interest for CTS in FTU was fruitfully tested in ECCD experiments on TRIAM-1M [37].

Considering the MW power level at which the ITER diagnostics will be operated, the constraints on the CTS antennas indicated by our results and the positive indications they provide in this respect quite straightforwardly extend to the perspective of α particle CTS in ITER.

6.3 Physics study of LH propagation

The analysis of the whole FTU data set on the LHCD efficiency, η_{CD}, has pointed out important parametric dependences on the major plasma parameters. The physical reasons for the experimental spread close to a factor 3 in the η_{CD} values have been recognized [38]. The main causes have been identified in the modifications suffered by the $N_{||}$ (parallel index of refraction) spectrum along the ray trajectory before the power is absorbed. The effect of the density fluctuations inside the edge turbulent layer crossed by the LH rays has been stressed being primarily of linear nature. However, also the presence of non-linear interactions should be considered, mainly those causing parametric decay instabilities (PDI) in the low frequency acoustic range and consequently modifying the $N_{||}$ spectrum entering the core. A numerical code, Lhstar on purpose recently developed [39], models the LH wave absorption in a tokamak, when edge PDI can grow. The $N_{||}$ spectral broadening occurring at the edge provides the bridge over the spectral gap necessary for absorbing effectively the LH power in the core, though it affects a small fraction of the power (~10%). The effect of the toroidicity in the main plasma is retained and, the ray tracing and the Fokker-Planck analyses are performed in parallel and consistently at each radial step of the calculation, for each ray. The calculated absorption profiles for JET are consistent with the measured q profiles [40].

7. Perspectives

A priority of the next FTU experimental campaigns will be the full testing of the liquid lithium limiter under strong additional heating (LH+ECH) and surface thermal load in excess of 10 MW/m^2. The stability of the liquid surface against disruption will also be assessed, and the new high density / high particle confinement regimes will be characterized in more detail. The study of ITB physics will be mainly focused on the ion transport under greater collisional coupling to electrons, by exploiting the full capability of the auxiliary heating systems in order to decrease the ratio $\tau_{ei,th}/\tau_E$, between the thermal e^--i^+ equipartition time and the energy confinement time, so far always larger than 5. This will be carried out mainly increasing density in discharges with plasma current $I_p \geq 0.5$ MA. The full automation and a complete feedback loop in the MHD stabilization by local ECCD is also in the future plans, as well as the restart of the IBW (ion Bernstein wave) radiofrequency system ($P_{IBW} \leq 0.5$ MW, f_{IBW}=433 MHz) for possibly inducing directly a poloidal velocity shear in the core plasma (r/a~0.5). Full exploitation of the recently installed motional Stark effect + charge exchange recombination spectroscopy diagnostic will provide essential information on the ion temperature and plasma current radial profiles. On the side of support to ITER issues, it is planned to investigate deeply the promising capabilities of ECH+LHCD systems in assisting the plasma start-up, to optimize disruption mitigation by ECH and to study more systematically the effect of LH on disruptions. The possibility of testing a new launching/ receiving antenna for the collective Thomson scattering is also being considered.

References

[1] Special Issue on FTU *Fus. Sci. Techn. (Guest editor C. Gormezano)* **V. 45** (May 2004)
[2] B. Angelini et al., *Nucl. Fusion*, **V. 45** (2005) p. S227-S238
[3] S. M. Kaye et al., *Nucl. Fusion*, **V. 37** (1997) p. 1303

[4] M. J. Greenwald et al., *Nucl. Fusion*, **V. 28** (1988) p. 2199
[5] V. Pericoli Ridolfini et al., *21st Fusion Energy Conf.*, Chengdu-China (2006), paper EX/P1-15
[6] V. Pericoli Ridolfini et al., *Plasma Phys. Control. Fusion*, **V. 47** (2005) p. B285–B301
[7] C. Gormezano et al., *Plasma Phys. Control. Fusion*, **V. 46** (2004) p. B435–B447
[8] J. Mailloux et al., *Phys. Plasmas*, **V. 9 No. 3**, p. 2156-2164 (2002)
[9] S. Ide et al., *Nucl. Fusion*, **V. 40**, p. 445-451 (2000)
[10] V. Pericoli Ridolfini et al., *Nucl. Fusion*, **V. 43** (2003) p. 469–478
[11] C. Sozzi, et al. *Journal of Physics: Conference Series*, **V. 25** (2005) p.198–209
[12] M. De Benedetti et al., *32nd EPS Conf. Tarragona* (2005), Europh. Conf. Abs., **V. 29C**, P4.035
[13] G. Granucci et al., "*Application of ECRH/ECCD on FTU: an Overview of Recent Results*", invited paper at 14th Workshop on ECE and ECRH, Santorini (Gr), 9-11 May 2006
[14] S. Cirant et al., *Journal of Physics*: Conference Series, **V. 25** (2005) 223–233
[15] J. Berrino et al., *Nucl. Fusion*, **V. 45** No 11 (November 2005) 1350-1361
[16] E. Lazzaro et al., *Phys. Rev. Lett.* **V. 84**, 6038 (2000)
[17] S. Cirant et al. 18th Fusion Energy Conf., Sorrento, Italy, (2000) paper EX3/3
[18] E. Lazzaro et al., 6th International Workshop "*Strong Microwaves in Plasmas*", Nizhny Novgorod, Russia, 2005
[19] J.N. Brooks et al., *Fusion Science and Technology*, **V. 47**, (2005) 669-677
[20] V.A. Evtikhin, I.E. Lyublinski, et al., *Fusion Eng. Des.*, **V. 56-57** (2001) 363-367
[21] V. Pericoli Ridolfini et al., "*Edge properties with the liquid lithium limiter in FTU - experiment and transport modelling*", submitted to PPCF.
[22] M.L. Apicella et al., "*First experiments with lithium limiter on FTU*", 17th PSI Int. Conf. Hefei, Anhui, China, 22-26 May 2006, to be published in J. Nucl. Mat.
[23] R. Zagórski, H. Gerhauser, *Physica Scripta*, **V. 70**, Part 2/3, (2004) 173
[24] G. Mazzitelli et al., *21st Fusion Energy Conf.*, Chengdu-China (2006), paper EX/P4-16
[25] F. Zonca et al., *21st Fusion Energy Conf.,* Chengdu-China (2006), paper TH/3-2
[26] K.L. Wong, et al., *Phys. Rev. Lett*., **V. 85** (2000) 996
[27] P. Smeulders et al., *29th EPS Conf., Montreux*, Europh. Conf. Abs. **V. 26B** (2002) D-5.016
[28] X.T. Ding et al., *Nucl. Fusion*, **V. 42** (2002) 491
[29] L. Chen et al., *Phys. Rev. Lett*., **V. 52** (1984) 1122
[30] B. Esposito et al., *33rd EPS Conf., Roma*, Italy, Europh. Conf. Abs. (2006) **V. 30I**, P5.071
[31] J.R. Martin-Solis et al., *Nucl. Fusion*, **V. 45** (2005) 1524
[32] J.R. Martin-Solis et al., *Nucl. Fusion*, **V. 44** (2004) 974
[33] J.R. Martin-Solis et al., "*Enhanced production of runaway electrons during disruptive termination of discharges heated with lower hybrid power in the Frascati Tokamak Upgrade"*, accepted for publication in Phys. Rev. Lett. (2006)
[34] H. Bindslev et al., "*ITER Fast Ion Collective Thomson Scattering – Feasibility Study*", Annex *1*, Riso Lab. Report, EFDA Contract 01.654, November 2003
[35] U. Tartari et al., *Nucl. Fusion*, **V. 46** (2006) 928 940.
[36] R. Prater et al. 10th Joint Workshop on ECE and CRH, Ameland (The Netherlands, 1997), Word Scientific, ISBN 981-02-3219-5, 531-540
[37] H. Idei et al., *Nucl. Fusion* **V. 46** (2006) 489
[38] V. Pericoli Ridolfini et al., *Nucl Fusion* , **V. 45** (2005) , p. 1386-1395
[39] R. Cesario et al., *Phys. Rev. Lett.,* **V. 92** , p. 175002-1-175002-4 (2004)
[40] C. Castaldo et al., *33rd EPS Conf*., Roma, Italy (2006), Europh. Conf. Abs., **V. 30I**, P1.122